Geophysical Journal (1988) **94,** 73–81

Sp phases from the Australian upper mantle

Günter Bock

Department of Geology and Geophysics, University of New England, Armidale, NSW 2351, Australia,

Accepted 1987 December 24. Received 1987 December 23; in original form 1987 July 6

SUMMARY

Routinely published source mechanisms of large earthquakes greatly facilitate the selection of data that may be suitable for the study of *S* to *P* conversions from the upper mantle. This is demonstrated for three stations of the Global Digital Seismograph Network located at Narrogin (NWAO), Charters Towers (CTAO) and Tasmania University (TAU) in Australia. Of ten events that were selected, eight showed precursors to *S*, *SKS* and *ScS* on long-period vertical-component seismograms at epicentral distances between 70° and 91°. The precursors are interpreted as *Sp* conversions from the upper mantle beneath Australia and surrounding areas. Synthetic seismograms that were calculated for the PREM model of Dziewonski and Anderson (1981) show good agreement with many details of the data. The main precursor arrivals are compatible with *S* to *P* conversions from a seismic discontinuity at 400 km depth. Relative to conversions from the '400-km' seismic discontinuity, *Sp* phases from the '670-km' discontinuity have much smaller amplitudes both in the synthetics and data in the epicentral distance range from 75° to 85°. It is suggested that *Sp* phases from the '670-km' discontinuity can best be observed at epicentral distances beyond 89°. This is confirmed by one observation at $\Delta = 90.6°$ made at CTAO. Within the limits of resolution of long-period data, there is no indication for strong lateral variations in the upper mantle discontinuity at 400 km between various geological provinces of Australia and surrounding areas. There are indications for the presence of *S* to *P* converted phases from a depth near 220 km. Their appearance is variable so that they are difficult to explain by *S* to *P* conversions at a seismic discontinuity at this depth.

Key words: *Sp* conversions, upper mantle, Australia, synthetic seismograms

INTRODUCTION

The transition between the upper and lower mantle is characterized by two major seismic discontinuities at depths near 400 km and 670 km (Dziewonski & Anderson 1981). The discontinuities are believed to be associated with phase transitions in the olivine system (e.g. Ringwood 1975) but, in the case of the '670-km' discontinuity, both a compositional change and phase transformation at this depth have been suggested by Lees, Bukowinski & Jeanloz (1983) to explain the inferred sharpness of the discontinuity. Numerous seismological investigations indicate that the two discontinuities in the transition zone exist worldwide but there may be lateral variations in sharpness (Faber & Müller 1984) and depth to the discontinuities (Paulssen 1985). A third seismic discontinuity in the upper mantle is located at about 220 km depth and is known as the 'Lehmann' discontinuity (Anderson 1979). Its nature is difficult to explain on the basis of currently accepted petrological models of the upper mantle (Leven, Jackson & Ringwood 1981). Leven *et al.* (1981) suggested that anisotropy as a result of alignment of olivine crystals in the direction of lithospheric plate movement causes the anomalously high *P*-wave velocities associated with the Lehmann discontinuity in Australia. This conclusion is challenged by Drummond, Muirhead & Hales (1982) who suggested—in agreement with Anderson (1979)—that the Lehmann discontinuity occurs worldwide.

Seismological investigations of the upper mantle have been based on three classes of observations: refraction seismic studies, underside reflections from mantle discontinuities, and converted phases. For an appraisal of the methods see Muirhead (1985). In view of the planned extension of the Global Digital Seismograph Network (GDSN) to a 100-station broadband network under the auspices of IRIS (Smith 1986) it is an attractive idea to use converted phases in mapping the sharpness and depth of seismic discontinuities in the mantle. On a continent-wide scale and within the limited resolution of long-period data, Faber & Müller (1980, 1984) mapped the transition zone under North and Central America, Europe, and East Asia. On a more local scale, Paulssen (1985) explained observations of *P* to *S* conversions beneath western Europe by depth variations of the '670-km' discontinuity. Faber & Müller pointed out that mode conversions in the depth range from 400 km to 700 km arriving as precursors to *S*, *SKS*, and *ScS* are best observed at epicentral distances between 70° and 100°. They also discussed the complications arising from the interference of *P* to *S* conversions in the source region with *S* to *P* conversions beneath the receiver making it difficult to separate source from receiver structure. Only in the special case of maximum *SV* and small *P*

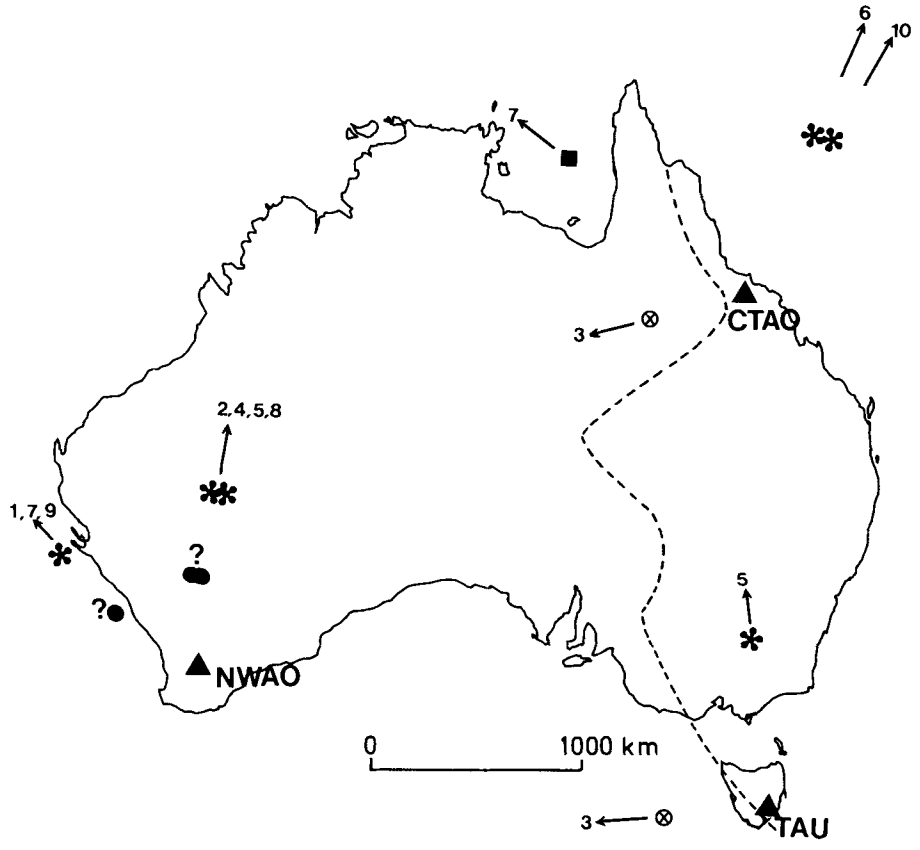

Figure 1. Location map showing GDSN stations used in this study as filled triangles and the inferred points of *Sp* conversions at depths of 220 km (dots), 400 km (asterisks) and 670 km (square). Crosses circumscribed by a circle denote areas that do not show conversions from the '220-km' discontinuity for an event located in the westerly azimuth of CTAO and TAU. Arrows show the approximate directions of events used in the study. The eastern limit of the Precambrian shield (after Howard & Sass 1964) is indicated by the dashed line.

radiation towards the station, mode conversions are mainly from *S* to *P* and can then be related to structure beneath the receiver.

The search for such favourable cases is considerably facilitated by the routine publication of moment tensor source solutions in the Preliminary Determination of Epicenters (PDE) bulletin of the US Geological Survey. It is the purpose of this paper to demonstrate the effectiveness of such an approach by describing the results of a search for *Sp* phase conversions originating in the upper mantle beneath Australia. The notation 'Sp_n' is frequently used in the paper to indicate *Sp* conversions near the receiver where '*n*' stands for the depth of conversion. The study focuses on long-period data of the three GDSN stations in Australia (Fig. 1) located at Narrogin in western Australia (NWAO), Charters Towers in Queensland (CTAO) and Tasmania University in Hobart (TAU). It is suggested that a systematic search for converted phases as described in this paper may be successfully applied to other GDSN stations as well.

DATA SELECTION

GDSN data used in this study were provided in the form of network-day tapes (Hoffman 1980). Events in the period 1984 January until 1985 October were selected on the basis of the centroid moment tensor (CMT) solutions (Dziewonski, Chou & Woodhouse 1981) published in the monthly PDE listings. The far-field radiation pattern was calculated from the parameters of the 'best double couple' derived from the CMT and the event was selected if it had good *SV* radiation towards Australia and the stations were located close to a nodal plane of *P*-waves. In addition, the stations had to be located at epicentral distances beyond 70° where *Sp* conversions from the upper mantle are likely to be best observed. Deep earthquakes (depth > 300 km) were not considered as seismic energy in the *P*-wave coda may interfere with *Sp* phases; for a more detailed discussion of this point see Sacks, Snoke & Husebye (1979) and Faber & Müller (1980). The selection resulted in 11 events that fulfilled all the above criteria. Of these only one, the Kurile Island event of 1984 December 17 proved to be unsuitable as surface waves from a foreshock interfered with body waves from the event. The focal parameters of the remaining 10 events are listed in Table 1.

OBSERVATIONS

The earthquake data recorded at CTAO, NWAO and TAU were extracted from the network-day tapes using software developed by Zirbes & Buland (1981). The time window was made long enough to include both *P*- and *S*-wave data. After data retrieval, the long-period horizontal components were rotated into the radial and transverse components. Fig. 2 shows vertical, radial and transverse seismograms at NWAO from seven events listed in Table 1. Three events recorded at TAU are shown in Fig. 3 and seismograms of five events recorded at CTAO in Fig. 4. Data quality at

Table 1. PDE parameters of earthquakes used in this study.

No.	Date	Origin Time UT	Epicentre		Depth (km)	m_b
			Latitude	Longitude		
1	1984 Feb 16	17-18-41.6	36.43°N	70.83°E	208	6.1
2	1984 Oct 14	03-18-31.5	46.15°N	152.68°E	33	5.9
3	1984 Nov 06	07-58-51.3	18.88°S	67.35°E	10	6.2
4	1984 Dec 03	04-08-35.1	44.21°N	148.14°E	65	6.4
5	1985 Mar 28	16-07-06.8	40.31°N	140.36°E	166	6.1
6	1985 May 24	22-04-43.4	51.42°N	178.43°W	34	5.8
7	1985 Aug 02	07-46-53.3	36.17°N	70.78°E	120	6.1
8	1985 Aug 12	03-49-18.0	37.77°N	141.77°E	52	6.0
9	1985 Aug 23	12-41-56.1	39.43°N	75.22°E	7	6.4
10	1985 Oct 09	09-33-32.4	54.76°N	159.61°W	30	6.2

CTAO and NWAO was generally satisfactory but of the TAU records only three had a sufficiently high signal to noise ratio to be of any value. Energy preceding the *S*-wave arrivals (throughout this paper, *S* is used in the sense $S + SKS + ScS$) is clearly visible on the vertical components of four NWAO records (events 1, 2, 4 and 5), one TAU seismogram (event 5) and three CTAO records (6, 7 and 10). Precursors to *S* do not stand out clearly on the remaining records, but they may be present for some events as indicated by question marks in Figs 2, 3 and 4.

Particle motion diagrams of which one example is shown in Fig. 5 did confirm that the *S* precursors are longitudinally polarized. Maximum peak to peak amplitudes of *P* and *SV* measured on the vertical and radial component respectively were used to form the amplitude ratios SV/P given in Tables 2, 3 and 4. Five of the ten events studied are associated with large SV/P ratios (>4) indicating that their focal mechanisms were indeed favourable for the generation of *Sp* phases. Two examples from CTAO (events 3 and 10) and one from TAU (event 8) have SV/P ratios between 2 and 4 indicating takeoff angles that are roughly 10–20° off the maximum of *SV* radiation. This is a crude estimation which depends very much on how close to a nodal plane the *P*-wave leaves the focus. The four records with SV/P ratios less than 2 suggest that in these cases the take-off directions of *S* may have been intermediate between the direction of maximum *SV* radiation and the *P* or *T*-axis.

INTERPRETATION AND DISCUSSION

The observed precursors to *S* are best explained by *S* to *P* conversion in the upper mantle beneath the receiver. However, other possible causes such as an incompletely decayed *P*-wave coda or *P* to *S* conversions in the source region can be ruled out. Ray-theoretical travel times of surface reflections that may carry significant seismic energy

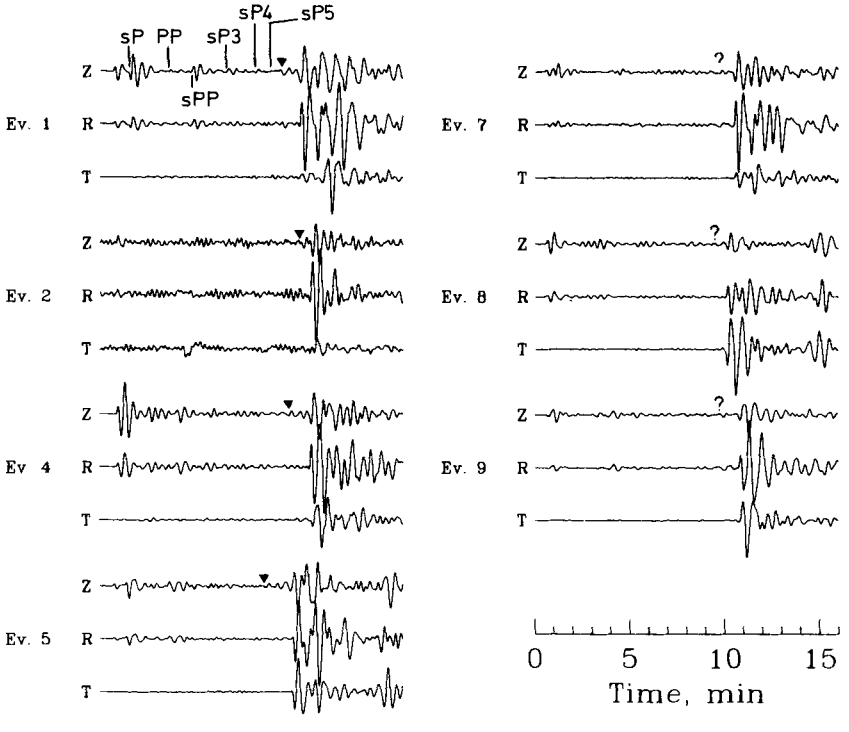

Figure 2. Long-period recordings of the vertical (Z), radial (R) and transverse (T) components at NWAO for events 1, 2, 4, 5, 7, 8 and 9. The onsets of *Sp* conversions from the mantle are marked by the inverted triangles.

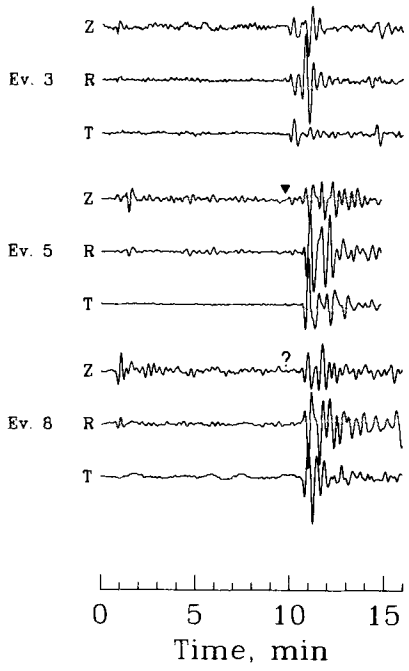

Figure 3. Long-period recordings of events 3, 5 and 8 at TAU.

in the coda of P were calculated on the basis of the Herrin (1968) P-model and the S-model of Randall (1971). In no case did the theoretical times of PP, PPP up to $P6$ fall near the precursor arrivals. Depth phases of the type sPn, where n stands for the number of P multiples were strongest from event 1 at NWAO but significant amplitudes were only observed for $n \leq 4$ (Fig. 2). Multiples with $n > 4$ appear to be sufficiently small in amplitude so that they do not interfere with S-wave precursors.

With a few exceptions, the amplitude ratios SV/P given in Tables 2–4 are large. This suggests that P to S conversions in the source region have negligible amplitudes and that the observed S-wave precursors are Sp conversions originating in the mantle near the receiver. The conclusion is supported by the fact that the S-wave precursors appear mainly on the vertical-component seismogram.

Synthetic seismograms were calculated with the reflectivity method for SV-waves developed by Kind & Müller (1975) and extended by Faber & Müller (1980) to allow for the calculation of converted phases at given discontinuities. The parameters of the double-couple point source were those of the 'best double couple' of the CMT solutions. The source time history was described by an analytical moment function whose derivative consists of approximately one sinusoid of period 25 or 30 s depending on the instrumental response. The PREM model of Dziewonski & Anderson (1981) at reference period 1 s was employed in the calculations. The only modification to PREM was the replacement of the average crust by a 35 km-thick continental-type crust. In addition, the shield model SNA of Grand & Helmberger (1984) was also investigated as it has a higher S-wave velocity contrast across the '400-km' discontinuity than PREM.

Synthetic seismograms for events 1 and 7 are shown in Fig. 6 together with the observed seismograms at NWAO. Despite the limited resolution of long-period data it is possible to distinguish in the synthetics Sp conversions from the '220-km' and '400-km' discontinuities. Amplitudes of Sp_{220} and Sp_{400} are distinct on the vertical component but less prominent on the radial component, in good agreement with the observation particularly of event 1. Sp phases from the '670-km' discontinuity have very small amplitudes both in the synthetics and observed seismograms. A similar observation was reported by Baumgardt & Alexander

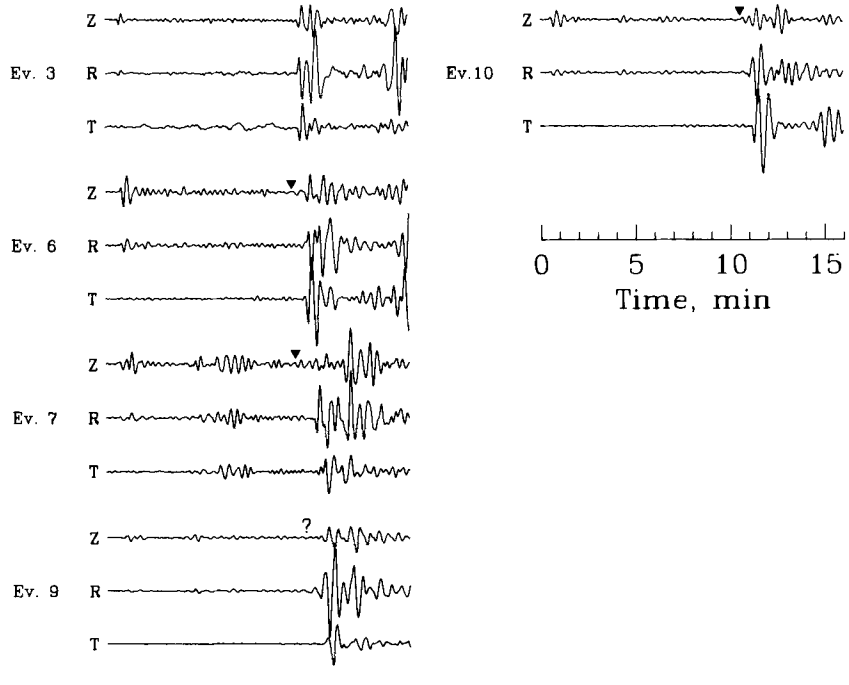

Figure 4. Long-period recordings of events 3, 6, 7, 9 and 10 at CTAO.

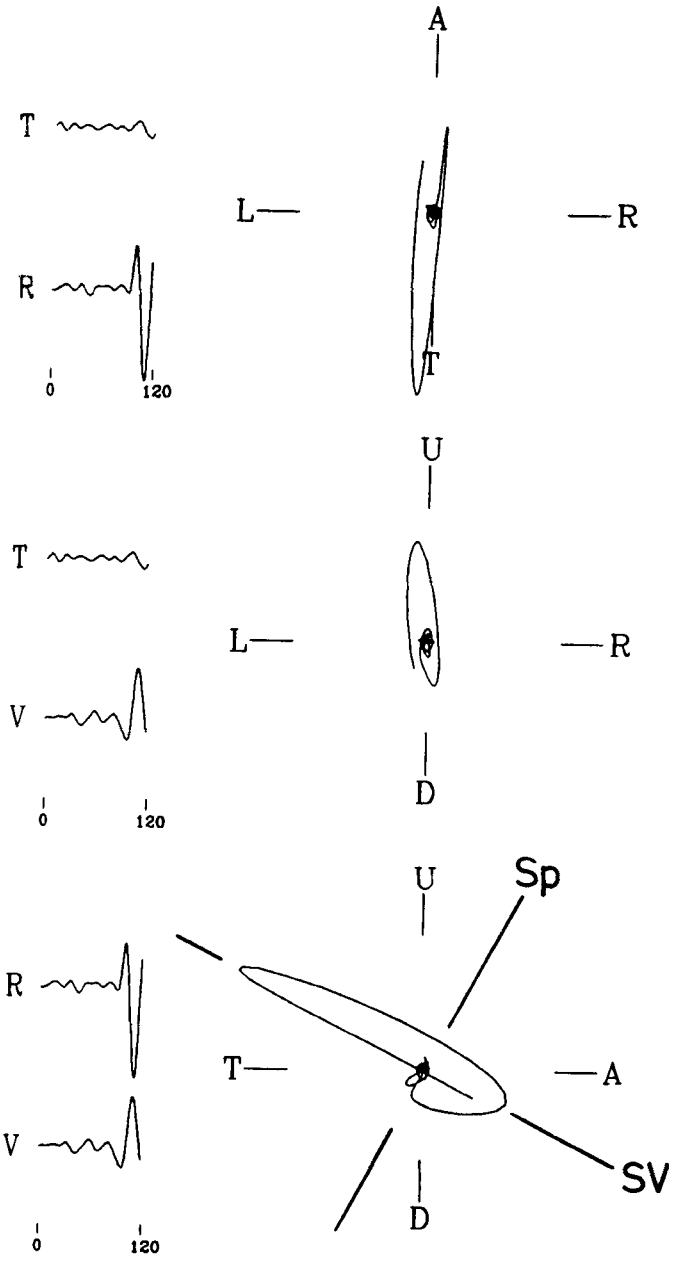

Figure 5. Particle motion diagram at NWAO for event 1 in the Hindu Kush over a 120 s long window including *S*-wave precursors and *S*-wave arrivals. Z, vertical; R, radial; T, transverse component. U, upward; D, downward motion at NWAO; A, motion away from; T, motion towards the source; R, motion to the right; L, to the left as seen from the source.

(1984) who studied mode conversions from the upper mantle beneath the LASA array.

The question of whether Sp_{220} is recorded at NWAO is difficult to answer. Synthetics were calculated for Sp_{400} and Sp_{670} only (Fig. 6e and f). Comparison of the PREM response with the shield model SNA reveals no significant differences between the two models. It thus appears that *Sp* phases from mantle discontinuities above 400 km contribute significant energy as precursors to *S*. However, there are two problems with this interpretation. Firstly, Sp_{220} arrives

Table 2. Amplitude ratios, epicentral distance Δ and station-to-epicentre azimuths at NWAO.

Event No.	*SV/P*	*Sp/S*	Δ, degree	Azimuth, degree
1	4.6	0.17	81.50	323.8
2	9.0	0.17	84.98	23.9
4	1.7	0.16	81.78	21.9
5	12.0	0.17	75.94	18.0
7	10.3	0.14	81.32	323.6
8	1.5	<0.16	73.96	20.0
9	5.0	0.12	81.85	328.4

P, *Sp* and *S* measured on vertical component; *SV* measured on radial-horizontal component

Table 3. Amplitude ratios, epicentral distance Δ and station-to-epicentre azimuths at TAU.

Event No.	*SV/P*	*Sp/S*	Δ, degree	Azimuth, degree
3	1.8		70.16	262.5
5	10.7	0.21	83.08	354.6
8	2.3		80.46	355.5

Table 4. Amplitude ratios, epicentral distance Δ and station-to-epicentre azimuths at CTAO.

Event No.	*SV/P*	*Sp/S*	Δ, degree	Azimuth, degree
3	3.6		73.67	255.6
6	1.6	0.17	77.64	21.7
7	7.0	0.67	90.57	308.4
9	11.5		88.82	312.9
10	3.5	0.13	87.66	28.0

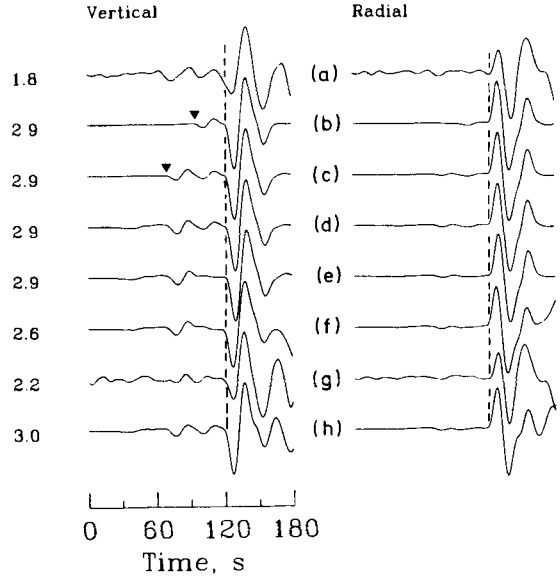

Figure 6. Observed S-wave seismograms at NWAO for events 1 (a) and 7(g) and synthetic seismograms. Based on the PREM model, *Sp* phases were calculated from seismic discontinuities at 220 km (b), 220 km + 400 km (c), 220 km + 400 km + 670 km (d and h) and 400 km + 670 km but without 220 km (e). Trace f shows synthetics for the SNA model in the upper 550 km of the mantle and PREM below with *Sp* phases from depths at 405 km and 670 km. The amplitude ratio of radial to vertical component is shown to the left of the traces. The onsets of *Sp* phases from the '220-km' (second trace from top) and '400-km' discontinuity (third trace) are marked by filled triangles. The onset of *S* is indicated by the dashed line.

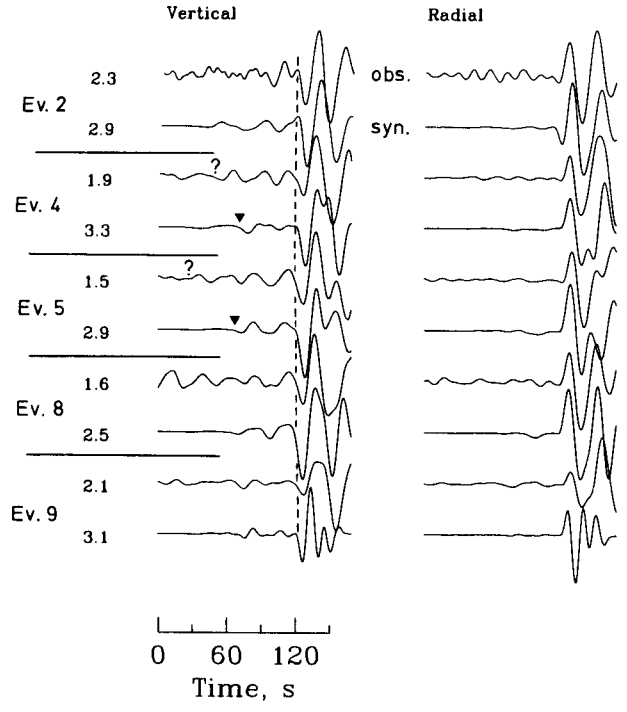

Figure 7. Observed (obs.) and synthetic (syn.) seismograms for events 2, 4, 5, 8 and 9 recorded at NWAO. The polarity was reversed for the observed seismograms from event 5 to enable trace alignment. Sp conversions were calculated from the discontinuities at 220 km, 400 km, and 670 km depth. In the synthetics, the onsets of the *Sp* phase from the '400-km' discontinuity are marked by a filled triangle for events 4 and 5. The onset of $S + SKS + ScS$ is indicated by the dashed line. Event number and the amplitude ratio of radial to vertical component are shown to the left of the traces.

in the coda of converted phases from deeper mantle discontinuities and is therefore more difficult to observe. Synthetic seismogram sections calculated for the distance range from 50 to 80° showed that Sp_{220} may best be observed at epicentral distances near 70°, where Sp_{400} has relatively small amplitudes. For NWAO, only event 8 was close to this favourable distance but unfortunately, this event had a less suitable source mechanism as indicated by the small SV/P ratio. Therefore, if Sp_{220} was produced at all its signal is likely to be lost in the *P*-wave coda (Fig. 7). The second problem is related to events 7 and 9 for which no clear *Sp* phases from the '220-km' discontinuity are visible (Figs 2 and 6) although they occurred in the same azimuth as event 1. The radiation pattern of event 7 was most favourable for the observation of *Sp* as the SV/P ratio is large and the *SV* waveforms are similar to those of event 1. No obvious explanation can be offered for the inconsistent appearance of *Sp* from these two events. Possible causes may be related to the assumed far-field displacement function used to produce the synthetics, interference of converted phases with a not completely decayed *P*-wave coda or *S* to *P* scattering in an inhomogeneous upper mantle near the receiver.

The observed precursors are consistent with *Sp* phases generated at the '400-km' and perhaps also at the '220-km' discontinuity. The maximum precursor-to-*SV* amplitude ratio for event 1 as measured on the vertical component is 0.15 for the synthetics which is slightly less than the observed ratio of 0.17, see Table 2. The difference can be explained by the fact that no corrections for absorption losses were applied to the synthetic *S*-wave seismograms. Faber & Müller (1984) estimate that *S*, *SKS* and *ScS* amplitudes are reduced roughly by 10 per cent relative to *Sp* as a result of differences in attenuation in the upper mantle beneath the receiver. Correcting the theoretical amplitude ratio by this factor results in good agreement with the observation.

Synthetic seismograms for the other five earthquakes recorded at NWAO are shown in Fig. 7. As for event 1, *Sp* phases from the '220-km' and '400-km' discontinuity dominate as *S*-wave precursors. Only for event 2 are converted phases from the '670-km' discontinuity visible in the synthetics but, as a result of a poor signal to noise ratio, they are not seen in the data. The synthetic *S*-waves from event 5 have polarities opposite to those observed at both NWAO and TAU indicating that the CMT solution in this case is erroneous.

Precursors preceding *S* by more than 60 s are present in the seismograms from events 4 and 5 at NWAO. Their approximate onsets are indicated by question marks in Fig. 7. It is unlikely that they are caused by *PS* conversions near the source because little energy shows up on the radial component. If they are *Sp* phases then the conversion depth is deeper than 400 km. *Sp* phases from the '670-km' discontinuity precede *S* by about 75 s but, in the synthetics, they have very small amplitudes indicating that they may be difficult to observe at epicentral distances less than 85°. As revealed by synthetic seismogram modelling, their amplitudes dominate those of *Sp* phases from shallower mantle discontinuities at distances beyond about 89°. The distance may be shifted towards smaller epicentral distaces if the '670-km' discontinuity dips downwards towards the receiver. Whether this is a valid model, however, cannot be decided on the basis of data from one station only.

Inspecting Fig. 7, it is obvious that, for event 4, the synthetic *Sp* phases bear little similarity with the observed seismogram. This may be a result of the focal depth chosen for this event. Precursors to both *S* and *sS* may interfere destructively to some extent if the *sS*–*S* differential time approaches the differential time of *Sp* phases originating from different discontinuities in the upper mantle. The effect of focal depth is illustrated in Fig. 8 where synthetic seismograms for different depths of the double couple point source are compared with the observed seismogram of event 4. For a depth of 60 km which is close to the PDE estimate Sp_{220} is reduced in amplitude as a result of interference with the *sSp* conversion from the '400-km' discontinuity. Reducing the depth to 35 km (which is the estimate published by the International Seismological Centre) is sufficient to produce a better match of synthetic with the observed seismogram, see Fig. 8.

Generally, many but not all of the details of the data are matched satisfactorily by the synthetics. Apart from the points just discussed, the precursor to *S* at NWAO from event 2 appears to be out of phase with the synthetic precursor. As mentioned earlier, this event was associated with a high noise level which makes it difficult to assess the significance of the phase shift. Another problem is related to event 9. Discrepancies in the frequency content become immediately obvious when comparing data and synthetic

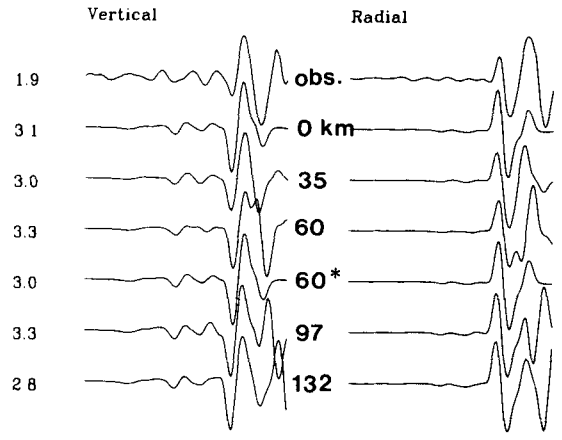

Figure 8. Observed (top) and synthetic seismograms for event 4 in the Kuril Islands. Synthetics were calculated for focal depths ranging from the surface to 132 km. Traces are aligned relative to the first minimum of the *S*-wave on the vertical component. The synthetic seismogram marked by an asterisk is for a focal depth of 60 km but depth phases are not included. Each trace is 180 s long. The numbers to the left of each trace give the amplitude ratio of radial to vertical component.

seismograms for this event (Fig. 7, see also Fig. 10). However, the appearance of Sp_{400} is satisfactorily matched by the synthetics. Summarizing the observations at NWAO, it is concluded that the observations of *Sp* phases from the '400-km' discontinuity can be explained by the PREM model. Conversions of the type Sp_{220} are not consistently observed which casts some doubt on the significance of the '220-km' discontinuity in a radially symmetrical earth model.

Similarly as just described for NWAO, the observations at CTAO and TAU were also compared with synthetic seismograms. Of the three events studied for TAU, only event 5 produced clear *S*-wave precursors. It is the event with the largest *SV*/*P* ratio (Table 3). The onset of *Sp* as marked in Fig. 3 can be associated with a conversion from the '400-km' discontinuity. There is no clear indication for a similar phase from event 8 which is located in the same

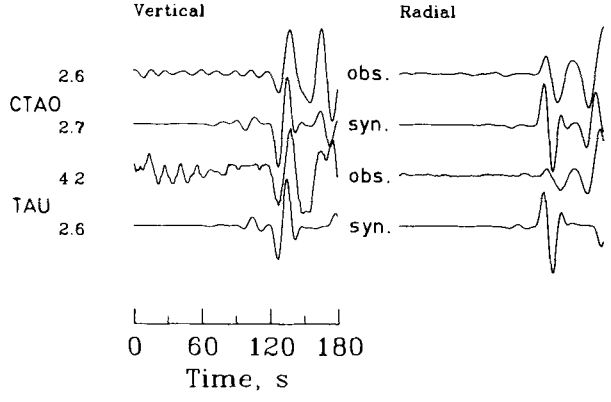

Figure 9. Observed (obs.) and synthetic (syn.) *S*-wave seismograms for event 3 recorded at CTAO and TAU from the westerly azimuth. *Sp* conversions were calculated from seismic discontinuities at 220 km, 400 km and 670 km depth. The synthetic vertical component clearly shows *Sp* phases from the '220-km' discontinuity but a similar phase is not seen in the data. Station code and the amplitude ratio of radial to vertical component are shown to the left of the traces.

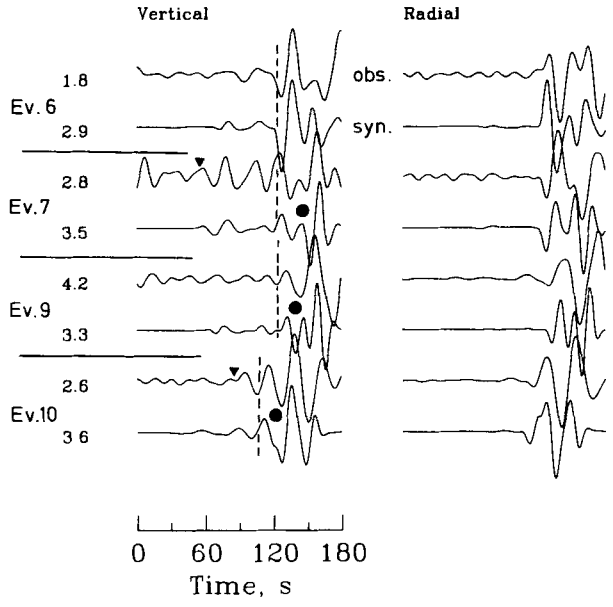

Figure 10. Observed (obs.) and synthetic (syn.) seismograms for events 6, 7, 9 and 10 at CTAO. *Sp* conversions were calculated from seismic discontinuities at 220 km, 400 km and 670 km depth. Events 7 and 10 were recorded at $\Delta > 87°$ and show *Sp* phases from the '400-km' (event 10) and '670-km' (event 7) discontinuities. Their approximate onsets are indicated by filled triangles. Event number and the amplitude ratio of radial to vertical component are shown to the left of the traces. The approximate onset of *SKS* (events 7, 9 and 10) and mantle *S* (event 6) is indicated by dashed lines. Dots mark the expected arrival times of mantle *S* and *ScS* for events 7, 9 and 10.

azimuth as event 5. This is probably the result of a less favourable source mechanism. Clearly, more data from TAU are required before any conclusions about the consistency of Sp_{400} at this station can be reached.

The TAU seismogram of event 3 was recorded at a distance of about 70° which, as mentioned earlier, is expected to be most suitable for the observation of Sp_{220}. There is no indication for such a conversion in the TAU record of the vertical component. Comparison of the observation with synthetics (Fig. 9) suggests that Sp_{220} should clearly stand out if PREM is the appropriate model. The theoretical ratio Sp_{220}/S is 0.17 as measured on the vertical component. Also shown in Fig. 9 are CTAO records of event 3 ($\Delta = 73.7°$) and the corresponding synthetics for PREM. The theoretical Sp_{220}/S ratio on the vertical component is 0.15 but no *S*-wave precursor of this magnitude is seen in the observed seismogram. Note that the ratio (noise preceding *S*)/*S* is about 0.10 on the vertical component of both TAU and CTAO.

Finally, the observations at CTAO will be discussed. Precursors to *S* are clearly seen on the vertical seismograms of events 7 and 10. Comparison with synthetics (Fig. 10) suggests that they are consistent with *SP* conversions from the '400-km' (event 10) and '670-km' (event 7) discontinuities near CTAO. In both cases, the occurrence of *Sp* is linked to mantle *S* and *ScS* while *SKS* produces only little precursor energy. For event 7, the amplitude of Sp_{670} is comparable to that of *SKS* on the vertical component. Relative to mantle *S*, the ratio *Sp*/*S* (Table 4) is large and about twice the synthetic ratio. This discrepancy may be

caused by constructive interference of *Sp* with phases in the *P*-wave coda or destructive interference of mantle *S* with *ScS* and *SKS* and does not necessarily imply a higher velocity contrast across the '670-km' discontinuity. A puzzling observation is that *S*-wave precursors from event 9 are visible on the radial component but less obvious on the vertical component. CTAO is located close to a nodal plane of event 9 as evidenced by both the CMT solution and the large *SV*/*P* ratio (Table 4) so that PS conversions in the source region are expected to contribute little precursor energy on the radial component. The synthetic for event 9 indicates that Sp_{400} and Sp_{670} may be present but, as a result of a high noise level on the vertical component, they do not stand out so clearly in the observation as in the cases of events 7 and 10. Still, the precursor on the radial component remains unexplained. *S*-wave precursors at CTAO that are present on the vertical component of event 6 may be consistent with the occurrence of Sp_{400} and Sp_{220}. With regard to the latter phase, the same problems as discussed earlier in relation to the observations at NWAO apply preventing a firm conclusion about the significance of the '220-km' discontinuity to be reached.

The locations of the conversion points in the upper mantle are depicted in Fig. 1. The horizontal distance from station to conversion point is about 4.5°, 8° and 9.5° for the '220-km', '400-km' and '670-km' discontinuities respectively. Five observations of Sp_{400} were made at NWAO. Conversions from events 4 and 5 took place in the Precambrian shield region of western Australia while the conversion points from events 1, 7 and 9 are located under the continental shelf of western Australia. The upper mantle conversion observed at TAU from event 5 took place in the Phanerozoic region of southeastern Australia. Further observations will show whether *S*-wave precursors at TAU from different events and azimuths are similarly consistent as they are at NWAO. Conversions from the '400-km' discontinuity observed from events 6 and 10 at CTAO occurred under the northern margin of the Coral Sea basin while the conversion from the '670-km' discontinuity observed from event 7 took place under the continental shelf region of the Gulf of Carpentaria. Within the limited resolution of long-period data, no significant lateral variations of the '400-km' discontinuity are indicated by the observations. Conversions from the '220-km' discontinuity may contribute to the precursor pattern observed at NWAO, but the observations are not consistent. The inferred conversion points of Sp_{220} are therefore shown with a question mark in Fig. 1. The two points depicted in Fig. 1 west to southwest of CTAO and TAU mark areas where *Sp* phases from the '220-km' discontinuity are absent as inferred from event 3.

CONCLUSION

The main emphasis of this study was put on the identification of *Sp* conversions from the Australian upper mantle. The search for events with good *SV* radiation towards the receivers is aided by earthquake source mechanisms that are now routinely published in seismological bulletins. The time-consuming and costly step of collecting data for the construction of fault-plane solutions is thus avoided. Of the events with good *SV* radiation towards Australia, most events showed clear precursors to *S* on the vertical-component seismograms that were interpreted as *Sp* conversions from the upper mantle near the receivers. Synthetic seismograms calculated for the radially symmetrical PREM model satisfactorily matched many but not all the details of the observations. Synthetics and data indicate that, in the distance range from 75° to 85°, *Sp* conversions from the '400-km' discontinuity dominate those from the '670-km' discontinuity. This explains the apparent absence of Sp_{670} at NWAO and TAU as the data from these stations were recorded at epicentral distances less than 85°. Events at distances greater than 89° are likely to be best suited for the study of *S* to *P* conversions from the '670-km' discontinuity.

Conversions from the '400-km' discontinuity took place under various regions of Australia and surrounding areas. Within the limited resolution of long-period data, there is no indication for strong lateral variations on the '400-km' discontinuity between these areas. A conversion from the '670-km' discontinuity was observed at CTAO from an event at a distance greater than 90°. The conversion point is located under the Gulf of Carpentaria.

With regard to conversions from the '220-km' discontinuity, theoretical seismograms for the PREM model predict amplitudes that are similar to those of Sp_{400} in the distance range from 75° to 85°. Towards smaller distances however, Sp_{220} is hardly disturbed by Sp_{400}. Seismograms recorded at CTAO ($\Delta = 73.7°$) and TAU ($\Delta = 70.2°$) from an event in the westerly azimuth provide no indication for the presence of converted phases from a discontinuity near 220 km which has the velocity contrast incorporated in PREM. On the other hand, observations at NWAO from events in the northerly azimuth are consistent with the presence of conversions from discontinuities located at depths near both 220 and 400 km while observations from the northwesterly azimuth provide no clear picture on the presence of Sp_{220}. The inconsistency of Sp_{220} speaks against simple refraction through a seismic discontinuity in a radially symmetrical earth model. It may be caused by scattering and conversions from *S* to *P* in an inhomogeneous upper mantle. Velocity anisotropy at the base of the continental lithosphere under the Australian shield as proposed by Leven *et al.* (1981) offers another alternative explanation for the sporadic occurrence of conversions from this depth. However, any such conclusions based on the data of this study should be avoided.

The sharpness of seismic discontinuities cannot be resolved to better than 50 km with long-period data. The Australian shield region is an area where short-period teleseismic *S*-wave arrivals have frequently been observed (Marshall, Douglas, Barley & Hudson, 1975; Hendrajaya, Muirhead & Bock, 1984; Bock & Ha, 1984). It is therefore an ideal place to study intermediate- and short-period *Sp* conversions from the upper mantle. Such observations could help to constrain the sharpness of upper mantle seismic discontinuities to better than 10 km and provide important constraints for petrological models of the upper mantle.

ACKNOWLEDGMENTS

Support by the Australian Research Grant Scheme is greatfully acknowledged. I wish to thank Madeleine Zirbes

for providing GDSN data and computer programs for data processing, Ken Muirhead for providing additional GDSN data, Brain Kennett for his radiation pattern program, Kevin Fleming for his help to prepare Fig. 5 and Gerhard Müller for critically reading an earlier draft of the manuscript.

REFERENCES

Anderson, D. L., 1979. The deep structure of continents, *J. geophys. Res.*, **84,** 7555–7560.

Baumgardt, D. R. & Alexander, S. S., 1984. Structure of the mantle beneath Montana LASA from analysis of long-period, mode-converted phases, *Bull. seism. Soc. Am.*, **74,** 1683–1702.

Bock, G. & Ha, J., 1984. Short-period *S-P* conversion in the mantle at a depth near 700 km, *Geophys. J. R. astr. Soc.*, **77,** 593–615.

Drummond, B. J., Muirhead, K. J. & Hales, A. L., 1982. Evidence for a seismic discontinuity near 200 km depth under a continental margin, *Geophys. J. R. astr. Soc.*, **70,** 67–77.

Dziewonski, A. M. & Anderson, D. L., 1981. Preliminary reference Earth model, *Phys. Earth planet. Int.*, **25,** 297–356.

Dziewonski, A. M., Chou, T. A. & Woodhouse, J. H., 1981. Determination of earthquake source parameters from waveform data for studies of global and regional seismicity, *J. geophys. Res.*, **86,** 2825–2852.

Faber, S. & Müller, G., 1980. *Sp* phases from the transition zone between the upper and lower mantle, *Bull. seism. Soc. Am.*, **70,** 487–508.

Faber, S. & Müller, G., 1984. Converted phases from the mantle transition zone observed at European stations, *J. Geophys.*, **54,** 183–194.

Grand, S. P. & Helmberger, D. V., 1984. Upper mantle shear structure of North America, *Geophys. J. R. astr. Soc.*, **76,** 399–438.

Hendrajaya, L., Muirhead, K. J. & Bock, G., 1984. Observations of the phase SP at distances less than 40°, *Geophys. J. R. astr. Soc.*, **78,** 307–312.

Herrin, E. (chairman), 1968. 1968 seismological tables for *P* phases, *Bull. seism. Soc. Am.*, **58,** 1193–1241.

Hoffman, J. P., 1980. The global digital seismograph network-day tape, *U.S.G.Surv. Open File Report,* **80–289**.

Howard, L. E. & Sass, J. H., 1964. Terrestrial heat flow in Australia, *J. geophys. Res.*, **69,** 1617–1626.

Kind, R. & Müller, G., 1975. Computations of *SV* waves in realistic earth models, *J. Geophys.*, **41,** 149–172.

Lees, A. C., Bukowinski, M. S. T. & Jeanloz, R., 1983. Reflection properties of phase transition and compositional change models of the 650-km discontinuity, *J. geophys. Res.*, **88,** 8145–8159

Leven, J. H., Jackson, I. & Ringwood, A. E., 1981. Upper mantle seismic anisotropy and lithospheric decoupling, *Nature,* **289,** 234–239.

Marshall, P. D., Douglas, A., Barley, B. J. & Hudson, J. A., 1975. Short period teleseismic *S* phases, *Nature,* **253,** 181–182.

Muirhead, K., 1985. Comments on 'Reflection properties of phase transition and compositional change models of the 670-km discontinuity' by Alison C. Lees, M. S. T. Bukowinski, and Raymond Jeanloz, *J. geophys. Res.*, **90,** 2057–2059.

Paulssen, H., 1985. Upper mantle converted waves beneath the NARS array, *Geophys. Res. Lett.*, **12,** 709–712.

Randall, M. J., 1971. A revised travel-time table for *S, Geophys. J. R. astr. Soc.*, **22,** 229–234.

Ringwood, A. E., 1975. *Composition and Petrology of the Earth's Mantle,* McGraw-Hill, New York.

Sacks, I. S., Snoke, J. A. & Husebye, E. S., 1979. Lithosphere thickness beneath the Baltic shield, *Tectonophys.*, **56,** 101–110.

Smith, S. W., 1986. IRIS: a program for the next decade, *Eos, Trans. Am. Geophys. Un.*, **67,** 213–219.

Zirbes, M. & Buland, R., 1981. Network-day tape software users guide version 3, *US Geol. Surv. Open-File Report,* **81–666**.